Chapter 1

The COMPASS Experiment

The COmmon Muon Proton Apparatus for Structure and Spectroscopy (COMPASS) experiment is a fixed target experiment at located on the French side at CERN. COMPASS started taking data in 2002 in the same hall as earlier Euopean Muon Collaboration (EMC), New Muon Collaboration (NMC) and Spin Muon Collaboration (SMC) experiments. COMPASS has studied hadron structure through (SI)DIS, Drell-Yan and Primakoff reactions and has done hadron spectroscopy measurements.

The COMPASS spectrometer is a two-stage spectrometer. The two stages are in a series and each stage contains various tracking detectors and as well at the end of each stage there is a muon wall filter for distinguishing between muons and other particles. Both stages also contain an electromagnetic and hadron calorimeter. Each stage is centerend around a strong spectrometer magnet used for determining particle momentum. The first stage downstream of the target is the large angle spectrometer (LAS) and it is centered around the SM1 magnet which has an integrated field of 1 Tm. This stage detects tracks with larger polar scattering angles roughly between 26 mrad and 160 mrad. The second stage is the small angle spectrometer (SAS) and it detects particle tracks having a scattering angle between roughly 8 mrad and 45 mrad. This stage is centered around the SM2 magnetic which has an integrated field of 4.4 Tm. A graphic of the 2015 setup is shown in Fig 1.1.

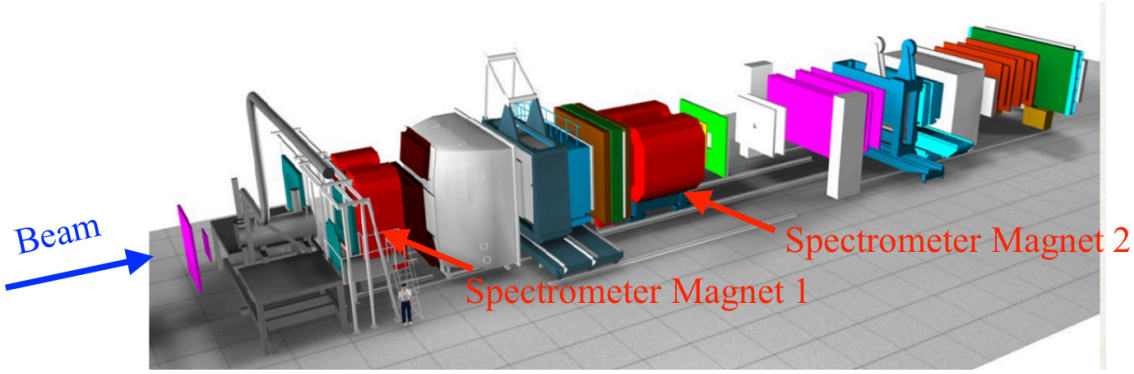

Figure 1.1: A schematic of the 2015 COMPASS setup

This chapter gives an overview of the COMPASS data taking setup with specific interest on the 2015 setup from which the data in this thesis was produced from. For a more thorough review of the spectrometer see reference [1]. This chapter is roughly organized by how the data taking occurs.

1.1 The Beam

The COMPASS spectrometer receives beam from the Super Proton Synchrotron (SPS) along on the M2 beam line. The Super Proton Synchrotron (SPS) is the second largest accelerator at CERN with a circumference of almost 7 km and it can accelerate protons up to an energy of 450 GeV. The SPS extracts beam to the Large Hadron Collier and as well sends beam to various experiments in the North Area at CERN. A schematic of the M2 beam line is shown in Fig. 1.2. There are several different beam types and energies available to COMPASS. The most common types used for physics analysis are a tertiary muon beam up to 190 GeV/c and secondary hadron beam with an energy up to 280 GeV/c. Both of these beam types can have a positive or negative charge. As well it is possible to have a lower intensity tertiary electron beam which is manly used for calibrations.

The start of the M2 beam line is the T6 target which is made of beryllium and has an adjustable length. The SPS accelerates primary protons up to 400 GeV/c which impinges on the T6 target to produce a secondary beam. The nominal proton intensity on the T6 target is 100x10^{11} spill^{-}1. The longer the T6 target the higher the secondary intensity where 500mm is the longest and typical target length used for physics data taking. The reaction of the proton beam with the T6 mainly produces secondary protons, pions and kaons. Following this reaction a series of dipole and quadruple magnets are used to select the momentum and charge of interest.

The SPS spill structure varies throughout the data taking year depending mainly on the needs of the Large Hadron Colider (LHC). In 2015 the average intensity provided was 0.6x10^{8} s^{-1} and the typical spill structure was two 4.8 second spills every 36 seconds.

1.1.1 Muon Beam

The muon beam is a tertiary beam which results from a weak decay of the secondary beam. After the initial proton reaction on T6 the resulting secondary particles are momentum and charge selected and sent through a 600m tunnel with focusing and de-focusing (FODO) quadruple magnets. In this tunnel the pion and kaons can decay as

$$\pi^{-(+)} \rightarrow \mu^{-(+)} + \overline{\nu}_{\mu^-}(\nu_{\mu^+}) \tag{1.1}$$

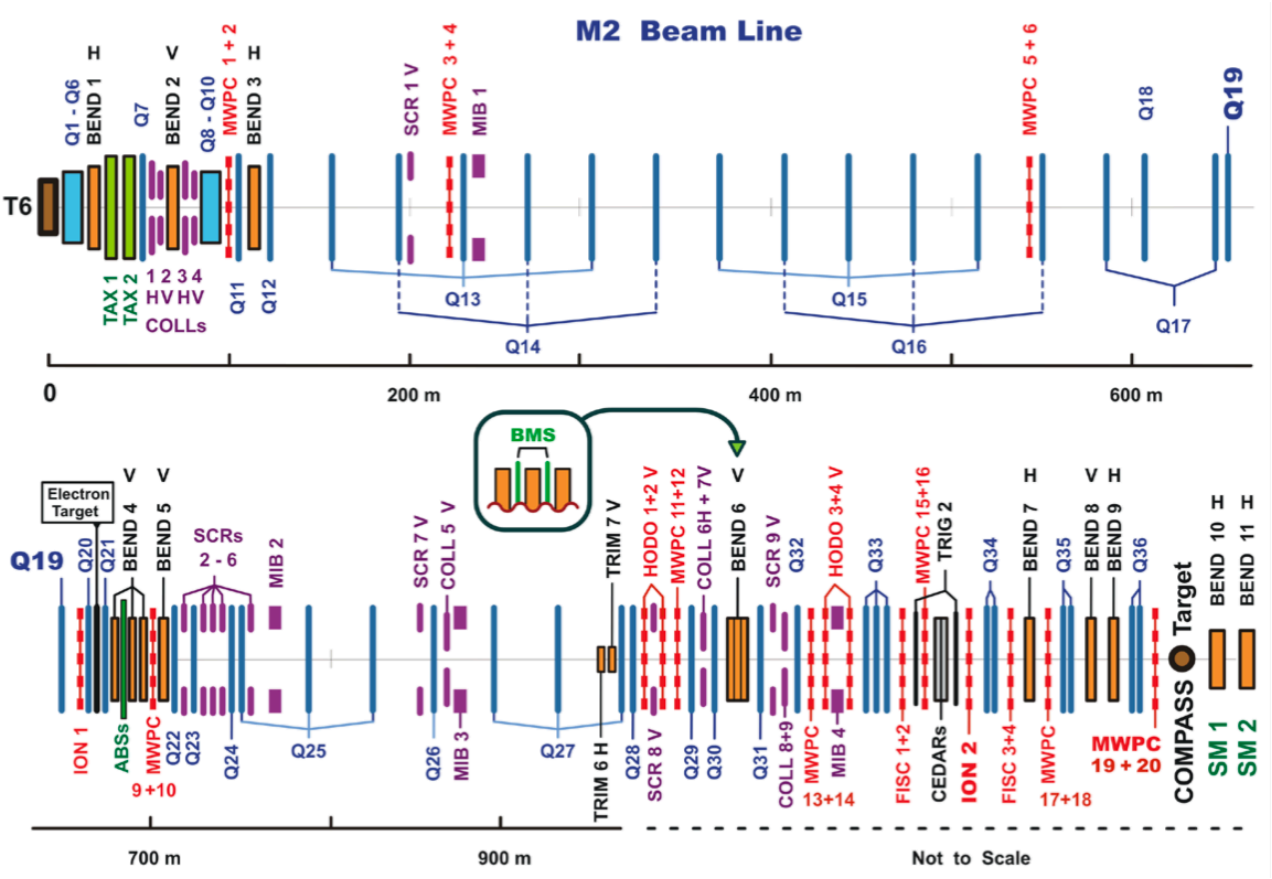

Figure 1.2: The M2 beam line at CERN

and

$$\kappa^{-(+)} \rightarrow \mu^{-(+)} + \overline{\nu}_{\mu^-}(\nu_{\mu^+}). \tag{1.2}$$

At the end of the tunnel a series of nine 1.1m long beryllium absorbers, referred to as the ABS in Fig. 1.2, remove the remaining hadron component of the beam which did not decay. A 172 GeV/c secondary beam is chosen to achieve a 160 GeV/c tertiary μ beam. Due to the fact that the neutrino in the reactions 1.1 and 1.2 is always left handed, the muon will be natural longitudinally polarized. For the muon momentum

chosen the muon beam achieves a polarization of 80%.

1.1.2 Hadron Beam

In the case of a hadron beam the ABS absorbers are not used and the decayed muons are removed due to their lower momentum. In the case of a negative hadron beam the composition of the beam is approximately 97 % π^-, 2.5% kaons and 0.5% $\bar{\text{p}}$. The 2015 Drell-Yan data taking used a 190 GeV/c hadron beam.

1.1.3 Additional Beam Line Components

After the decay tunnel the beam is bent upwards along another FODO tunnel of length 250m before reaching the surface approximately 100m before the COMPASS target. A series of three dipole magnets, called bend 6, then bend the beam to a horizontal position aimed at the COMPASS target. Both upstream and downstream of bend 6 are three tracking detectors (BM01-BM06) that make up the Beam Momentum Station (BMS). The BMS is the upstream most component of the COMPASS spectrometer and is able to determine the beam momentum to better than 1% of the beam momentum with an efficiency of approximately 93%. Bend 6 and the BMS are shown schematically in Fig. 1.3.

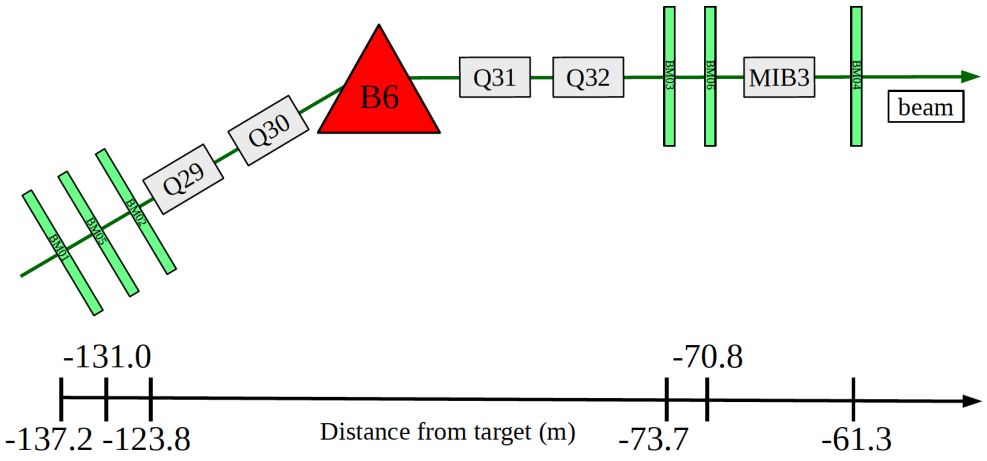

Figure 1.3: Bending the beam to a horizontal position. The BMS detectors are upstream and downstream of the bend 6 magnet.

For the 2015 Drell-Yan setup the π^- beam intensity was too high for the BMS station to work properly. For this reason special low intensity, approximately 10^6 s^{-1}, π^- beams were used in 2014 to determine the momentum distribution for Drell-Yan data taking. The beam momentum distribution is shown in Fig. 1.4 where the average momentum is 190.9 GeV/c with a spread of $\pm$ 3.2 GeV/c.

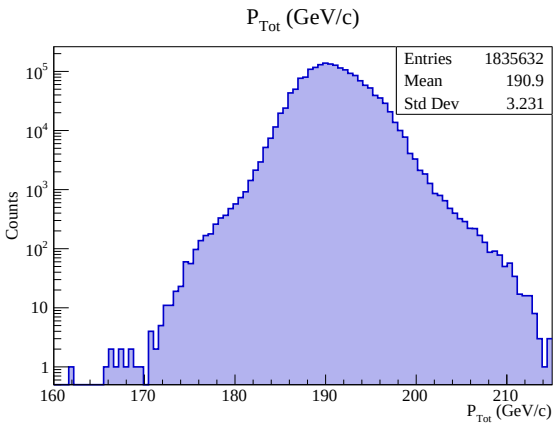

Figure 1.4: The momentum distribution of the π^- beam, determined during dedicated low intensity beam times.

Approximately 30 m upstream of the target are to two Cherenkov counters (CEDAR) detectors. As the hadron beam has contamination from several components these CEDARs can be used to distinguish between these components. The CEDARs at COMPASS are high pressure detectors and have been demonstrated to achieve fast particle identification for particle momentums up to 300 GeV/c. The general principle of operation for the CEDARs is that two particles with the same momentum but different mass will emit Cherenkov radiation at different angles relative to there momentum. When a particle is traveling faster than the speed of light in a given medium it emits Cherenkov radiation in a cone centered along its momentum axis. The faster the particle is traveling the narrower the angle of the Cherenkov light cone. A schematic of the CEDAR operating principle is shown in Fig. 1.5. In 2015 the CEDARs were measured to be largely inefficient due to the high beam intensity.

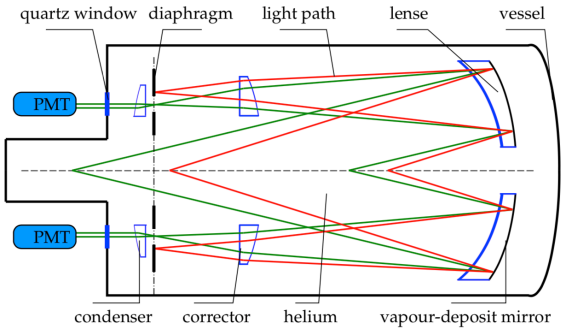

Figure 1.5: General principles of operation for the CEDARs at COMPASS. The red(green) lines correspond to Cherenkov light emitted from a particle.

For years with a transversely polarized target, such as 2015, a chicane system of dipole magnets is setup in front of the target. This is because a beam hitting the target without any angle would then be deflected

inside the target to the left or right of the spectrometer. For this reason the chicane gives the beam an angle before hitting the target such that the non-interacting beam exits the target traveling straight towards the spectrometer.

1.2 The Polarized Target

The polarized target at COMPASS is the most complicated and essential component of the spectrometer. It is located upstream of the tracking detectors and spectrometer magnets and downstream of the beam telescope, described in section 1.3, detectors. The target consists of 2 or 3 cylindrical cells and the possible materials are either solid state ammonia (NH_3) or deuterated lithium (^{6}LiD) or liquid hydrogen. Fig. 1.6 shows a schematic of the target.

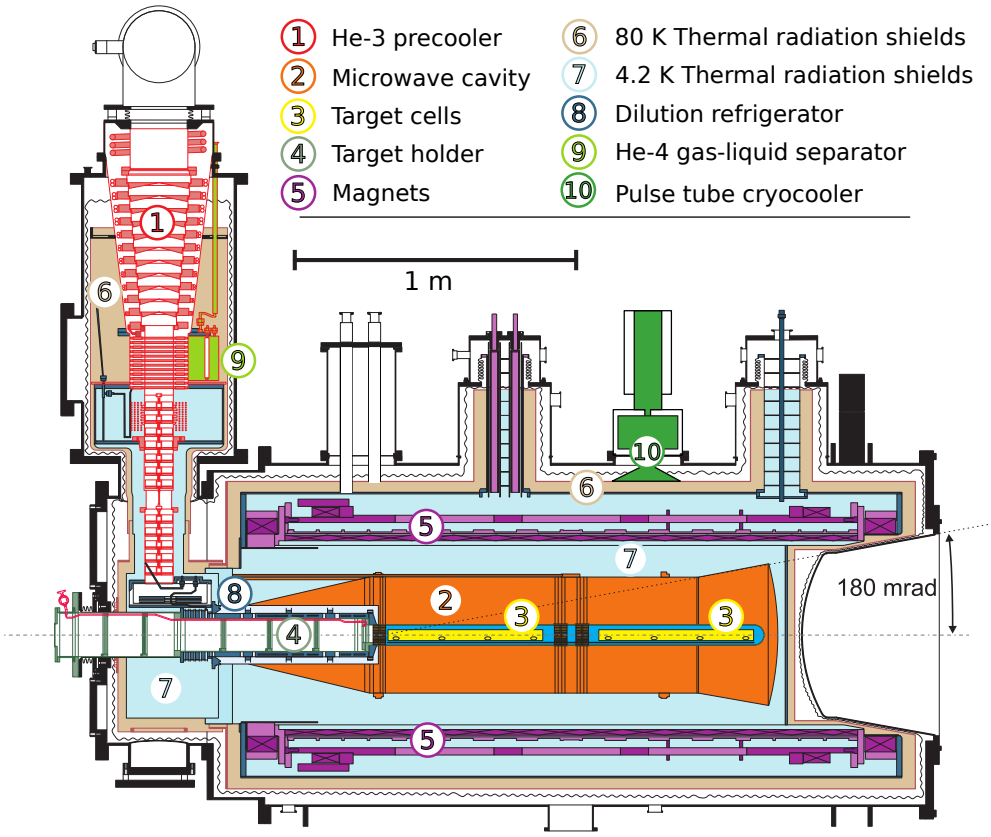

Figure 1.6: The polarized target at COMPASS

Surrounding the cylindrical cells is a longitudinal super conducting magnet capable of reaching a magnetic field of 2.5T. This longitudinal magnet polarizes the target in the direction of the beam momentum and the target polarization is maintained by keeping the target in a liquid helium bath of approximately 60mK. This

is called frozen spin mode where the temperature is maintained by a dilution refrigerator.

The target is polarized through the dynamic nuclear polarization (DNP) method [2]. This process works by first polarizing electrons in the target with the longitudinal magnet in the same longitudinal direction for all target cells while sending electromagnetic radiation in the microwave spectrum into the target. Due to their much lower mass, electrons have a larger magnetic moment and therefore can be polarized at a much faster rate than protons or neutrons. For atoms which have a nuclear spin it is then possible for these atoms to absorb a microwave going to an excited state with the electron spin anti-parallel to the magnet and the nuclear spin either parallel or anti-parallel to the magnet depending on the microwave frequency. The electron with the anti-aligned spin will then quickly have its spin realigned while the nucleon will take much longer to lose its polarization due to its smaller magnetic moment. This process can continue in this way resulting in a net nuclear polarization. Using the DNP method the target can achieve a polarization of approximately 90% in three days.

The target also includes a 0.63T transverse dipole magnet to change from longitudinal polarization to transversely polarized. The target must first be longitudinally polarized before the transverse target magnet can change the polarization direction. Once the target is transversely polarized, the target polarization can no longer be increased as microwaves can no longer shine on the target in the polarization direction. Therefore the polarization will decrease exponentially. In 2015 the target was polarized for about half a day between data taking sub-periods and achieved and average polarization of 0.73% which includes the effect of exponential polarization lose with time. The target transverse polarization relaxation time was about 1000 hours in 2015.

The target polarization was measured with 10 NMR coils while in longitudinal magnet mode. In the 2015, each target cell had the most upstream and downstream coils in the center of the target cell and the other three coils on the outside perimeter of the target cells. Due to the fact that the polarization can only be measured with the longitudinal magnet on, the polarization is only measure at the start and finish of a transversely polarized data taking. The intermediate polarization are then determined by exponential interpolating between these two times.

In 2015 the setup was two transversely polarized target cells of 55 cm length and 2 cm in radius, separated by 20 cm and oppositely polarized. The polarization of the target cells was flipped ever two weeks of data taking to reduce systematic effects. Due to the fact that the beam needs to be precisely steered onto the target anytime a beam line magnet is changed and that the chicane magnets upstream of the target are setup for only one transverse target direction, the transverse target magnet only pointed downward in 2015. To achieve a polarization flip the target polarization had to therefore be rotated back to the longitudinal

direction and the input microwaves had to be changed to achieve the desired polarization direction.

The target material in 2015 was NH_3 where the protons in the three hydrogen atoms were the only nucleons with nuclear spin. Therefore only some fraction of the target was able to be polarized and one would expect that this fraction is 3/17. However to get a more accurate determination of the dilution factor the follow calculation was used

$$f = \frac{n_H \sigma^{DY}_{\pi^- H}}{n_h \sigma^{DY}_{\pi^- H} + \sum_A n_A \sigma^{DY}_{\pi^- A}}, \tag{1.3}$$

where f is the dilution factor, n_H is the number of hydrogen atoms in NH_3, n_A is the number of other nucleons in NH_3, and $\sigma^{DY}_{\pi^- H}$ and $\sigma^{DY}_{\pi^- A}$ are the Drell-Yan cross-section for pion hydrogen scatter and pion nucleon scattering respectively. The cross-section were determined using a parton-level Monte-Carlo program MCFM [4]. The dilution factor was also further scaled down by studies of reconstruction migration between target cells. The average dilution factor in 2015 was 0.18.

1.3 Tracking Detectors

The goal of the tracking detectors is to determine a point in space where a particle traversed. The COMPASS tracking detectors attempt to do this for a wide range of angles, momentums and at different rates. For these reason there are several planar tracking technologies used at COMPASS which can be divided into three categories: very small angle tracker, small angle trackers and large area trackers. As the name suggest very small angle trackers measure tracks with small angle deflections from the beam axis which are essentially beam particles. The small area trackers measure particle tracks with low but non-zero angle have central dead zones. The large area trackers are several meters in height and width and measures the largest deflection angles up to 180 mrad.

All of these trackers are split into stations where each station corresponds to several detectors at roughly the same z-position along the beam line. Each station measures a track position in one or more orientation while most measure tracks in three or more orientations. The coordinate orientations measured are the X and Y coordinates which are the horizontal and vertical directions respectfully and as well the U and V coordinates which are rotated at different angles with respect the X and Y coordinates.

1.3.1 Very Small Angle Trackers

The very small angle trackers extend up to 3 cm away from the beam axis. This is the region with the highest number of tracking particles and therefore these detectors must be able to handle the highest rates up to 5x10^7 Hz. The two detector types that make up the very small angle trackers are either scintillating

fiber detectors (SciFi) or silicon microstrip detectors. These two detector types are complementary to each other as the former have very good timing resolution while the latter have very good spacial resolution.

There are three silicon stations possible at COMPASS with active detecting areas of 5x7 cm^2. The spacial resolution of these detectors is nominally 10 μm and the timing resolution is nominally 2.5 ns. For the 2015 setup, the beam intensity was too high for the silicon detectors to operate and therefore these detectors were not used in 2015.

There are 10 SciFi stations available at COMPASS with sizes varying from 3.9x3.9 cm^2 to 12.3x12.3 cm^2 planar areas. The fiber diameters vary between detectors and are 0.5 nm, 0.75 nm and 1 nm. Several fibers are bundled together to determine a strip hit position and the resulting nominal spacial resolutions are 130 μm, 170 μm and 210 μm. The nominal timing resolution of these detectors about 400 ps. In 2015 three SciFi stations made up the beam telescope and were placed upstream of the target to measure the beam trajectory and timing information. A fourth SciFi station was place in the LAS section of the spectrometer.

1.3.2 Small Angle Trackers

The small angle trackers are small area detectors that detect particles with a non-zero defection angle. They cover 5 cm to 40 cm from the beam axis where the rate drops two orders of magnitude relative to the very small angle trackers to approximate 10^5 Hz. At COMPASS there are two types of small area tracking detectors: micromesh gaseous structure (micromegas) and gas electron multipliers (GEMs).

There are three micromega stations at COMPASS all location sequentially after each other between the target and the first spectrometer magnet. All three detectors measure four coordinate projections and have an active area of 40x40 cm^2 with a 5 cm diameter dead zone. The micromegas operate by having a conversion region and a smaller amplification region. An ionized particle produced in the conversion region will drift through an electric field too small for amplifaction of around 3.2 kV/cm to the amplification region where the electric field is around 50 kV/cm and is high enough to amplify the sign which is then read out on strips. The conversion and amplification regions are separated by a metallic micromesh material. The electrons pass through the micromesh without resistance and are not rimmed out. The micromegas have good spacial resolution because the thickness of the amplification region is only 100 μm which is small enough to prevent the electron avalanche from spreading out much transversely between strips. The separation of the larger conversion region from the smaller amplification region with the micromesh prevents electric field lines from being distorted in the conversion region and therefore prevents the primary electrons from drifting slower in the conversion region. This allows micromegas to operate at a higher rate than would be possible otherwise. This principle of operation is illustrated in Fig. 1.7. The strips in the central part of the detector are 360 μm

corresponding to a resolution of about 100 μm and the strips in the outer region are 460 μm corresponding to a resolution of about 120 μm. The nominal timing resolution 9 ns. In 2015 the micromegas were upgraded to include a pixelized section covering much of the dead zone area.

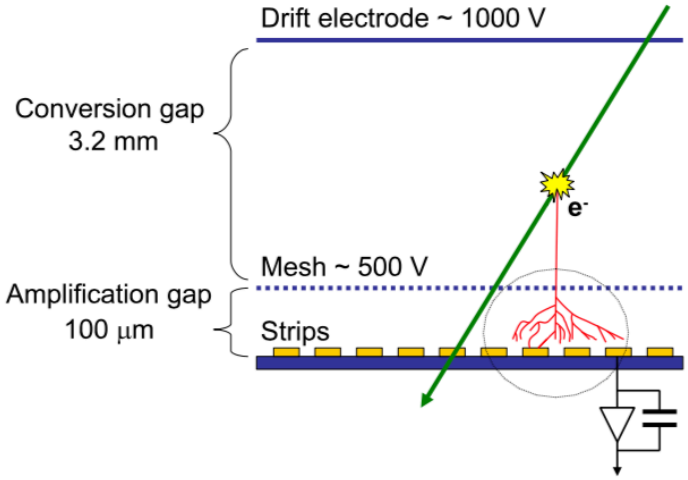

Figure 1.7: Principle of operation for the micromesh gaseous structures (micromegas)

There are eleven GEM detectors located throughout the COMPASS spectrometer starting after the first spectrometer magnet down to the end of the spectrometer. These detectors are close to the beam axis and are mounted on a large area tracker covering the dead zone region of the large area tracker. All eleven detectors have an active area of 31x31 cm^2 and a 5 cm diameter dead zone. In times of lower beam intensity the dead zones can be turned on as an active area. The detector is split into four regions separated by a polymide foil (50 μm thick) clad with copper on both sides with around 10^4 cm^{-1} drifting holes of 70 μm diameter. There in an electric potential of a few hundred volts between each foil layer. The GEM detectors speed up the amplification process by splitting the amplification avalanche into three locations there by allowing for a higher rate of operation then would otherwise be possible. The electron amplification occurs around the holes of each of the three foil dividers which therefore speeds up the overall drift time from the ionization location to the strip readout. This principle of operation is shown in Fig. 1.8. The nominal timing and spacial resolution of the GEM detectors is 10 ns and 110 μm respectively. Two pixelized GEM detectors where also in operation but were not as crucial for the 2015 Drell-Yan measurement.

1.3.3 Large Area Trackers

The large area trackers measure the largest polar scattering angles at COMPASS. Their dead zones mostly coincide with a small area tracker, described in the previous section 1.3.2, which therefore means these

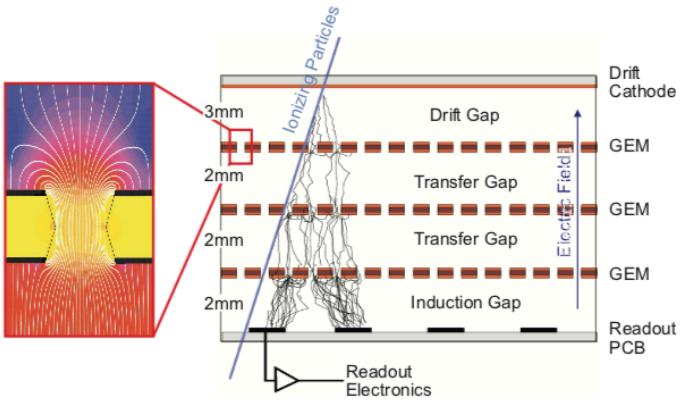

Figure 1.8: The operation principle of the gas electron multiplier (GEM) detectors

detectors do not have to process the higher fluxes very close to the beam line. The most important feature of these detectors is that they have a large planar area but as a consequence their position and timing resolution is not as good as the small and very small angle trackers. The types of large area trackers used are COMPASS are all gaseous detectors and include drift chambers (DCs), straw tube detectors (straws) and multi-wire proportional chambers (MWPCs).

The first four drift chambers downstream of the target are named DC00, DC01, DC04 and DC05. The first two, DC00 and DC01, have smaller active areas of 180x127 cm^2 and a circular dead zone of 30 cm diameter and are positioned upstream of the SM1 magnet. The rates upstream of SM1 are higher due to low energy particles produce in the target, which are bent out of the acceptance of spectrometer by SM1. Therefore DC00 and DC01 need to be able to process a higher particle flux. The next two drift chambers, DC04 and DC05, are downstream of SM1 and both have larger active areas of 240x204 cm^2 and as well have dead zones of 30 cm diameter. The active areas of all four of these DCs was roughly chosen to coincide with the acceptance of the SM1 yoke. DC05 was first installed for the 2015 Drell-Yan data taking and is further described in chapter **??**. All four of these DCs measure four projection views corresponding to eight detector layers. A sketch of the principle of operation is shown in Fig. 1.9. The nominal spacial resolution for these detectors is 250 μm.

There are additional drift chambers downstream of the SM2 magnet, named W45. W45 consist of six detector stations which each have an active area of 520x260 cm^2 and a circular dead zone of 50 cm or 100 cm diameter. Each W45 station measure two projection views corresponding to four detector layers. The drift cells in W45 are 40x10 mm^2 and the spacial resolution is nominally 1500 μm.

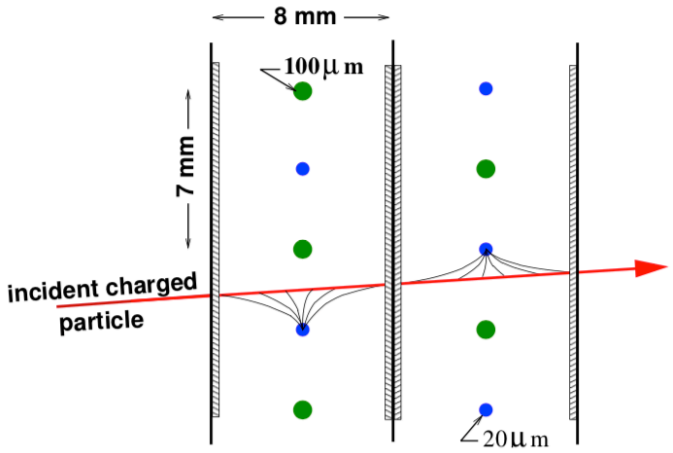

Figure 1.9: Drift cell of a Drift chamber with the ionized drift electron lines coming from the incident charged particle

In 2015 there were two straw stations in operation named ST03 and ST05. ST03 was in the large angle spectrometer after DC05 and consisted of two stations measuring six projection views. ST05 was in the small angle spectrometer and measured three projection views. The active areas of horizontal wire stations is 350x243 cm^2 and the active area of the rotated wires is 323x272 cm^2. The principle of operation for the straw detectors is very similar to that of a drift chamber however instead of having the detector made up of connected drift cells the straw detectors are made of circular tubes. Each tube consist of a gold plated tungsten anode wire in the center and the walls of the tube make up a cathode. Due to the fact that the cathode completely surrounds the anode wire there is no electrical interference between neighboring anode wires as there is for drift chambers. For this reason the electric field in each tube is easier to control and the ionized electron drift speed is more linear than other detectors. Each straw detector plane is divided into sections where the straw tubes in the outer most section from the beam line have a diameter of 9.6 mm and the tubes close to the beam line have a diameter of 6.1 mm. In additional in the central part of the detector there is a physical hole dead zone of 20x20 cm^2. The nominal position resolution for these detectors is 400 μm and a frontal schematic is shown in Fig. 1.10. For the reason that most of the final state muon are reconstructed in the large angle spectrometer and the fact that many of the high voltage modules were not operation for ST05 in 2015, ST05 was not used for track reconstruction for Drell-Yan data.

Another large area tracker that operates similarly to the straw tube detectors is the richwall detector. This detector is located before the SM2 magnet and after ST03 with an active area of 5.27x3.91 cm^2 and a central dead zone of 1.02x0.51 cm^2. The detector consist of eight layers of mini drift tubes (MDT) shown in

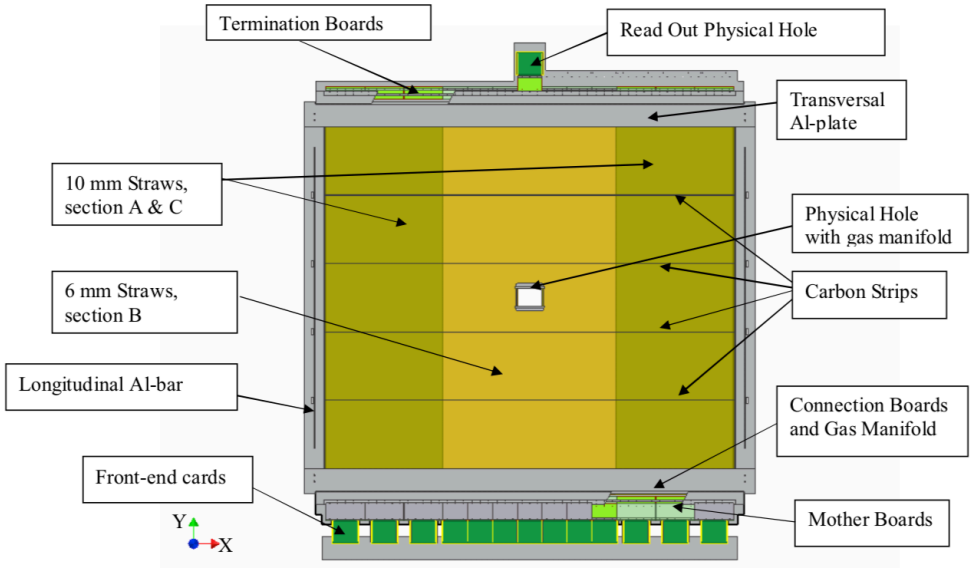

Figure 1.10: Front on view of a the active area of a straw detector at COMPASS

Fig. 1.11. The central part of each MDT includes a gold plated tungsten sense wire. The nominal position resolution of this detector is 600 μm.

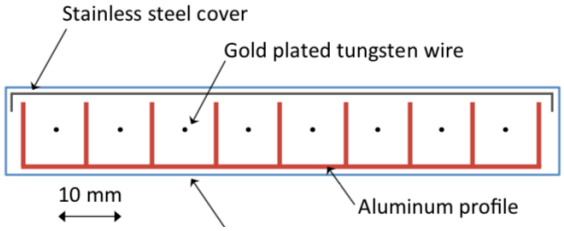

Figure 1.11: The richwall mini drift tubes

The final type of large area tracking detector at COMPASS is the MWPC. There are 14 of these stations located throughout the experiment. These MWPCs are separated into three categories distinguished by the coordinates they measure. The first type is called type A and consists of three projection views measuring an x, u and v coordinate. The second type is type A* and is the same as type A but measures the y coordinate in addition to the other three coordinates. Both type A and A* have active areas of 178x120 cm^2. The final type is type B which has a smaller active area of 178x90 cm^2 and measures the same projections at type A. There are seven stations of type A, one station of type A* and six stations of type B. All three types have circular dead zones of diameters 16 cm, 20 cm and 22 cm for types A, A* and B respectively.

The MWPCs operate on similar principles to the drift chambers but without a calibration drift curve.

For this reason the MWPCs can be made to have one common gas volume between each station and their position resolution is determined as

$$\frac{\text{sense wire separation}}{\sqrt{12}}. \tag{1.4}$$

The separation between sense wires is approximately 2 mm which corresponds to a spacial resolution of these detectors around 600 μm.

1.4 Particle Identification

In the COMPASS spectrometer there are four types of detectors used to determine particle identification (PID): the ring image Cherenkov (RICH) detector, electromagnet calorimeters (ECAL), hadron calorimeters (HCAL) and muon walls (MW). The RICH distinguishes between pions, kaons and protons; ECAL1 and ECAL2 measure the energy from photons and electrons; HCAL1 and HCAL2 measure the energy from hadrons; and MW1 and MW2 distinguish muons from all other particles. The RICH, ECAL1, HCAL1 and MW1 are in the large angle spectrometer in that respective order along the beam line. The small angle spectrometer includes ECAL2, HCAL2 and MW2 again in that respective order along the beam line.

The RICH detector operates similarly to the CEDARS, section 1.1.3, in that Cherenkov radiation is emitted from particles traveling through the RICH at an angle dependent on their velocity. The RICH is filled with a dielectric gas, C_4F_{10} which as an index of refraction greater than air. The momentum of particle going through the RICH is determine from bending angle around SM1 and therefore the mass of particles can be distinguish once the RICH determines the entering particles velocity. A sketch of the RICH and its operating principle is shown in Fig. 1.12. To distinguish between particles the minimums momentums are: 2.5 GeV/c for pions, 9 GeV/c for kaons and 17 GeV/c for protons. The maximum momentum the RICH can distinguish between any of these particles is 50 GeV/c. This detector is located in the large angle spectrometer before any calorimeters.

The ECALs and HCALs both stop specific particles of interest where the energy deposited in each respective calorimeter is proportional to the incoming particle's energy. This energy knowledge along the momentum determined from the tracking detectors allows to determine particle identification. The ECALs and HCALs can therefore measure the energy of incoming particles. The ECALs are made of lead glass towers with photon multipliers attached to these towers on one side. An incoming photon or electron interacts with the lead glass to produce a light signal which is readout with these photon multipliers. Other particles also interact with the material in the ECALs however hadrons and muons are able to exit through the detector

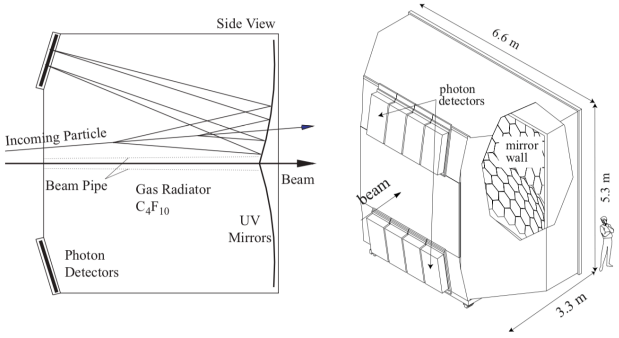

Figure 1.12: Side view demonstrating the principle of operation of the RICH detector.

unlike photons and electrons. A frontal view of ECAL1 is shown in Fig. 1.13 and a frontal view of ECAL2 is shown in figure Fig. 1.14.

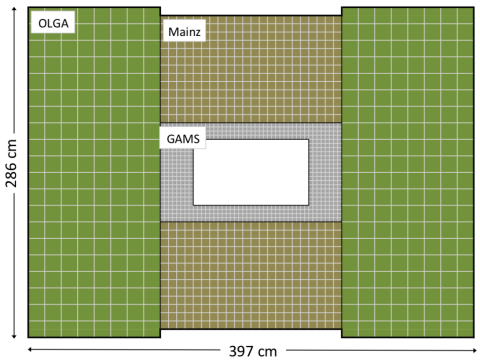

Figure 1.13: Frontal view of the electromagnetic calorimeter 1

The HCALs are sampling calorimeters which are made of alternating layers of iron and scintillating material. An incoming hadron deposits all its energy in the HCAL by making a particle showers in the iron which are detected by photo multipliers connected to the scintillating material. The HCALs are placed after the ECALs in each stage of the spectrometer because an electromagnetic shower happens faster than a

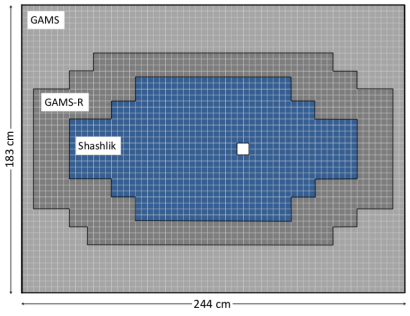

Figure 1.14: Frontal view of the electromagnetic calorimeter 2

hadronic shower. The HCALs are affect at determining particles energy from particle with energies between 10 GeV and 100 GeV.

The two MWs are located after an HCAL in their respective stages. Due to their higher mass and absence of color charge, muons are able to pass through the most material budget of any of the particles detected at COMPASS. For this reason both MWs consist of an absorber and tracking detectors downstream of this absorber. Any particles that make it through the absorber are with a very high probability muons. MW1 consists of eight tracking planes before a 60 cm iron absorber and same number of tracking planes after this absorber. The tracking portions of MW1 are build similarly to the richwall, described in section 1.3.2, in that they are also made of MDT modules. The active area of MW1 is 480x410 cm^2 and includes a dead zone of 140x80 cm^2. Each plan of this detector has a spacial resolution of 3 mm. A sketch of MW1 is shown in Fig. 1.15. The second muon wall, MW2, is located downstream of a concrete absorber which 2.4 m thick. MW2 consists of 12 planes with and active area of 450x450 cm^2 and a dead zone of 90x70 cm^2. The detector operates similarly to the straw detectors, section 1.3.2, in that it is made of drift tubes with a wire in the center of these tubes. The diameter these drift tubes is 29 mm and the position resolution is about 1.4 mm.

There is one last absorber in the COMPASS spectrometer located before the H5 hodoscope at the end of the spectrometer hall. This absorber is called muon filter 3 (MW3) and ensures that the inner trigger is only triggered by a muon.

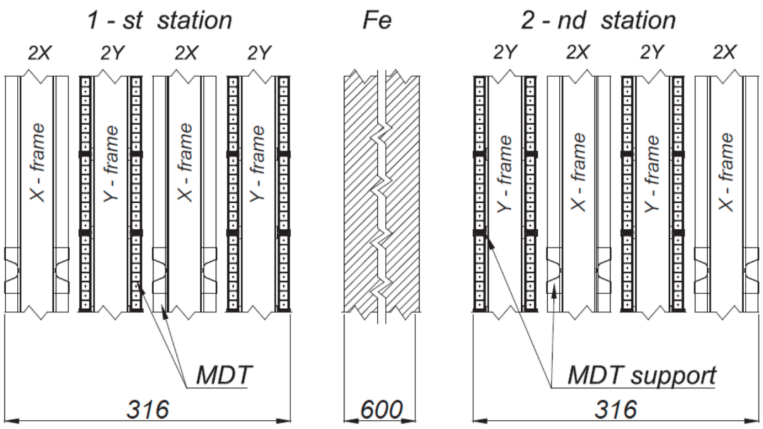

Figure 1.15: A side view sketch of the muon wall 1 detector

1.5 Trigger

The trigger system at COMPASS defines what is an event. Whenever the trigger signal is given, all the detector information within a few nanosecond timing window is recorded. Due to the fact that there are very many background events occurring as the beam impinges on the target, there is too much information going to the front end modules (FEMs) of the detectors for the FEMs to process and record all the information. For this reason only a certain subset of all the information is stored to disk. The trigger system must therefore have good timing resolution to make quick decisions on which data to record. At COMPASS a system of scintillating hodoscopes attached to PMTs is use as the trigger. The timing resolution of these detectors is approximately 1 ns. A top view schematic of COMPASS showing where the relative position hodoscopes for each trigger is shown in Fig. 1.16.

At COMPASS there are five different triggers used to register physics events. Each trigger type includes at least two hodoscopes at different z-positions in the spectrometer. The types of triggers are either target pointing, when the hodoscope slabs are horizontal; or energy loss, when the hodoscope slabs are vertical. The target pointing trigger is setup used with higher polar scattering angles to signal an event if a particle is scattered from the target and the energy loss trigger is setup used with lower Q^2 interactions to signal an event if a particle is bent a specified amount. This concept is illustrated in Fig. 1.17. There are four triggers in SAS: the inner trigger (IT), the middle trigger (MT), the ladder trigger (LT) and the outer trigger

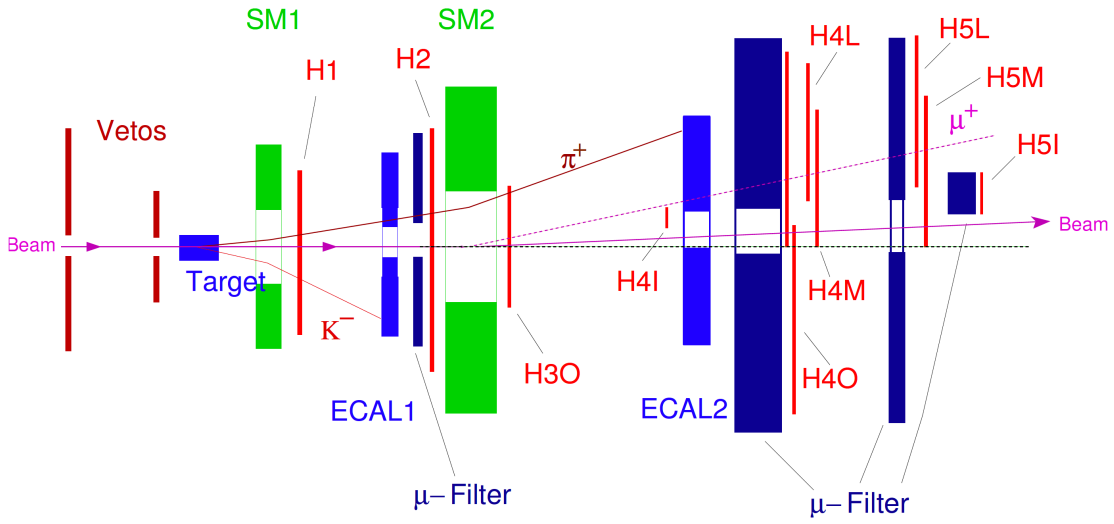

Figure 1.16: Top view of the spectrometer highlighting how different particles can signal a trigger

(OT). The IT is an energy loss trigger and includes the hodoscopes HI04X and HI05X. The MT includes both energy loss and target pointing slabs. The hodoscopes in the MT are HM04X, HM05X, HM04Y and HM05Y. The MT hodoscopes whose names end with an X have vertical slabs and those ending with a Y have horizontal slabs. The LT is an energy loss trigger which consists of HL04X and HL05X. The final trigger in SAS, the OT, is a target pointing trigger and consists of hodoscopes HO03Y and HO04Y. The remaining trigger system is in LAS and is a target pointing trigger consisting of hodoscopes HG01Y and HG02Y.

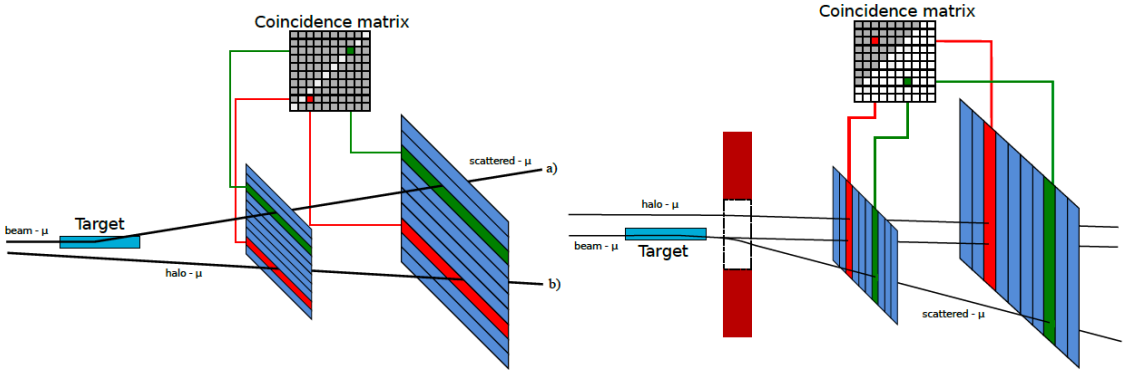

Figure 1.17: The two types of triggers (left is target pointing and right is energy loss) at COMPASS and an illustration of the coincidence matrix used to select events of interest

There is also a veto system upstream of the target as shown in Fig. 1.16. This veto trigger consist of hodoscopes attached to PMTs as well. It is centered on the beam axis but with not active area in the nominal beam line. The veto trigger is used to reject halo muons. Halo muons occur from the beam decaying, as in

Eq. 1.1 and Eq. 1.2, where this decay occurs upstream of the target but downstream of the ABS absorbers. The muon halo surrounds the hadron beam due to its lower momentum which allows the veto hodoscopes outside of the beam line to reject these type of events.

In addition to the five trigger systems based on hodoscopes is the calorimeter trigger (CT). The CT can be used as a trigger when a particle deposits more than a certain energy threshold in one of the calorimeters. In 2015 this trigger was only used as an independent study of the other triggers at COMPASS.

In 2015 setup the Drell-Yan process of interest corresponds to two detected muons. For this reason two triggers must signal a particle in coincidence for an event to be registered. For physics analysis the coincidence triggers are either two muons in LAS (LASxLAS), one muon in LAS and one in the OT (LASxOT) or one muon in LAS and one muon in the MT (LASxMT). The LASxLAS trigger system covers the high Q^2 and high x_{beam} phase space and the triggers including a SAS hodoscope cover lower Q^2 values. In addition to these three dimuon triggers where three single muon triggers corresponding to a particle in LAS, MT or OT. These three triggers however where pre-scaled down to only take every 500, 100 or 100 events respectively. For further tests 2015 included a random trigger and a beam trigger which was scaled down by 35000.

1.6 Data Acquisition

The data acquisition (DAQ) collects data from the over 250,000 detector channels and transfers this data to storage on magnetic tape at CASTOR (CERN Advanced STORage). Despite the triggering system used to reduce the data rate, the data rate ranges from 10 kHz to 100 kHz with a typical event size of 45 kB. The DAQ is designed handle these rates and data size while minimizing the dead time associated with data collection and transfer.

Data collection begins with the digitization of information from a detector channel eight by a time to digital converter (TDC) or an analogue to digital converter (ADC). These TDCs and ADCs are eight on the detector FEMs or on custom COMPASS readout electronics named: GANDOALF (Generic Advanced Numerical Device for Analog and Logic Functions), GeSiCA (Gem and Silicon Control and Acquisition) or CATCH (COMPASS Accumulate Transfer and Control Hardware). After digitization the data is transferred by optical fibers to an FPGA multiplexer where the data is buffered by spill and arranged by event. From there an FPGA switch sends the data to multiplexer slaves. The slaves are online computers that oversee the final steps for raw data and transfer this data to CASTOR. This whole process is show schematically in Fig. 1.18.

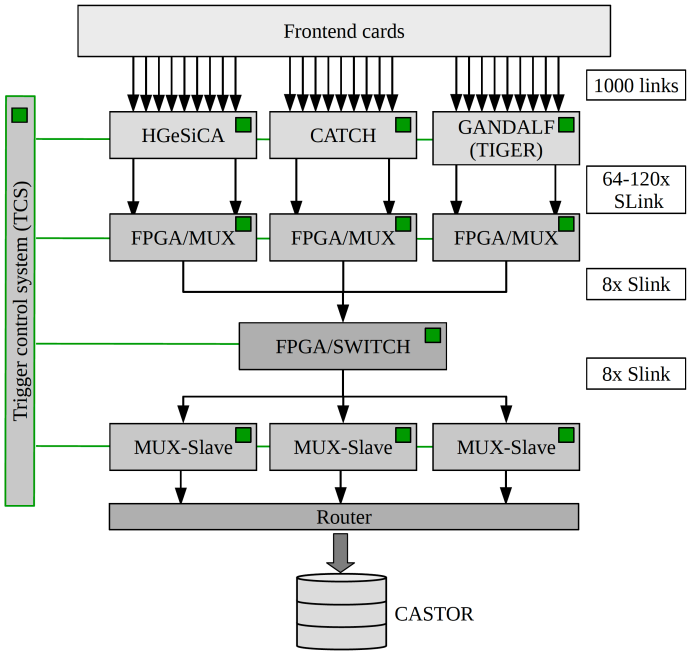

Figure 1.18: The data acquisition steps at COMPASS

1.7 Data Reconstruction

The COMPASS Reconstruction and AnaLysis Program (CORAL) reconstructs the raw data into physical quantities such as particles with momentum and charged and possibly an originating vertex location [3]. The raw data from the DAQ is digitized timing information from tracking detectors or digitized energy information for calorimeters. The process of reconstructing tracks takes the timing information and determines a position in space for a particular tracking detector based on a calibration. CORAL then uses a Kalman Filter to determine straight tracks in regions with no or low magnetic field [5]. The tracks are then connected through the magnetic field using a fast lookup table for known possible bending radii. At this point a track is determined to have a momentum, charge and a χ^2 value associated with the track. From there the tracks are extrapolated back to the target region and the intersect of two tracks is determined as a vertex. If in addition to the two intersecting tracks a beam particle can be extrapolated forward to the same vertex location then the vertex is assigned to be a primary vertex otherwise the vertex is defined as a secondary vertex. A diagram of the reconstruction data flow is shown in Fig. 1.19.

Once reconstruction has been performed the data is stored in data structured trees (DSTs). The usual procedure of reconstruction which gives physical values momentum and charge to tracks results in data called miniDSTs. There is the possibility to save more information, for example detector hit location information, to make so called fatDSTs. These DSTs are now in a format which can be processed by PHAST (PHysics

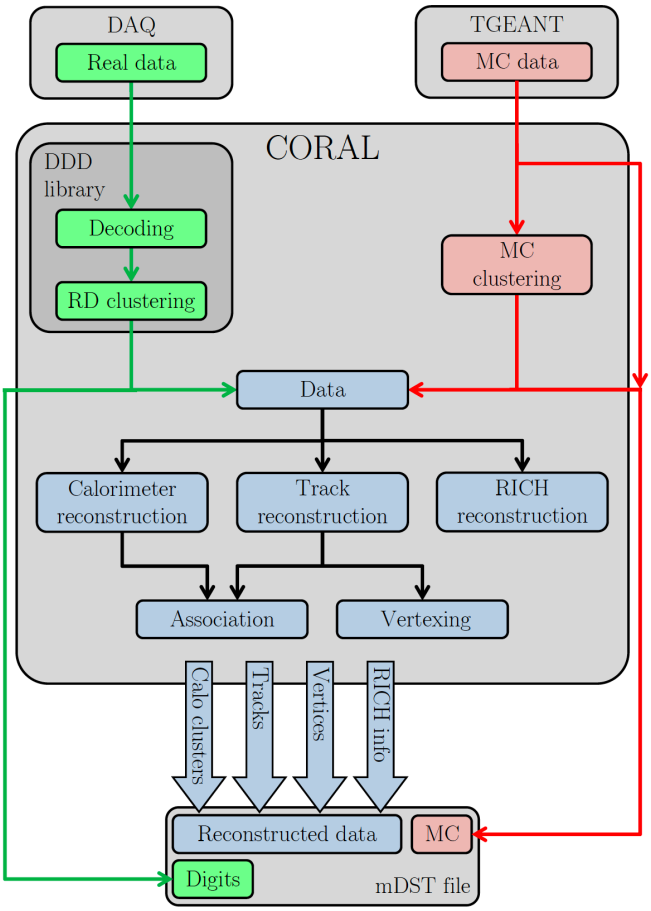

Figure 1.19: The schematic of the CORAL reconstruction process

Analysis Software Tool) which is COMPASS program written to further analyze physics data. With PHAST there is the possibility to loop over all the miniDSTs and make certain cuts to produce so called μDSTs. Both CORAL and PHAST are fully object-oriented C++ programs.

1.8 2015 Drell-Yan Data Taking

Both SM1 and SM2 have magnetic fields in the vertical direction meaning charged particles are deflected in the x-z plane and can therefore have their momentum determined. For beam reconstruction there is a beam telescope upstream of the target consisting of eight planes of scifi detectors. To account for the transverse magnetic field in the polarized target a chicane magnet system was added in the beam line. This meant that the beam entered at a slight angle in the beam telescope but exited the target going straight.

In 2015, COMPASS took nine data periods labeled W07-W15. Each data period lasted two weeks and the spin orientation of the targets was reversed after the first week of every period to reduce systematic

effects arising from different geometric acceptances and luminosities of up and downstream target cells.

For the 2015 Drell-Yan data taking a hadron absorber, see figure **??**, was placed just downstream of the target cells. This was done to reduce the amount of hadrons and electrons detected in the spectrometer and therefore ensured a cleaner di-muon sample. The absorber material was mostly alumina (Al_2O_3) and concrete and the absorber corresponded to approximately 7.5 interactions lengths of material. Inside the absorber was an aluminum target followed by a tungsten plug, each of radius 2.5 cm, which acted as a beam dump. The aluminum target and tungsten plug served the double purposes as absorbers and also as unpolarized nuclear targets. In addition a thin ^{6}Li absorber was added just downstream of the primary absorber to absorb thermal neutrons produced in the primary absorber. This ^{6}Li absorber was proposed to improve the performance of the first tracking detector downstream of the target.

1.8.1 DAQ and Reconstruction

The data acquisition system (DAQ) was recording events at a rate of approximately 30 kHz with a dead time of 10%. In 2015, COMPASS recorded approximately 750 terabytes of raw data from the nine, two-week periods. Raw data refers solely to individual detector timing and wire or strip positions and does not correspond to physics observables of interest. From this raw information the CORAL reconstruction software at COMPASS is able to determine the trajectory and momentum of charged particles going through the COMPASS spectrometer.

List of Figures

1.1 A schematic of the 2015 COMPASS setup . . . 1
1.2 The M2 beam line at CERN . . . 3
1.3 Bending the beam to a horizontal position. The BMS detectors are upstream and downstream of the bend 6 magnet. . . . 4
1.4 The momentum distribution of the π^- beam, determined during dedicated low intensity beam times. . . . 5
1.5 General principles of operation for the CEDARs at COMPASS. The red(green) lines correspond to Cherenkov light emitted from a particle. . . . 5
1.6 The polarized target at COMPASS . . . 6
1.7 Principle of operation for the micromesh gaseous structures (micromegas) . . . 10
1.8 The operation principle of the gas electron multiplier (GEM) detectors . . . 11
1.9 Drift cell of a Drift chamber with the ionized drift electron lines coming from the incident charged particle . . . 12
1.10 Front on view of a the active area of a straw detector at COMPASS . . . 13
1.11 The richwall mini drift tubes . . . 13
1.12 Side view demonstrating the principle of operation of the RICH detector. . . . 15
1.13 Frontal view of the electromagnetic calorimeter 1 . . . 15
1.14 Frontal view of the electromagnetic calorimeter 2 . . . 16
1.15 A side view sketch of the muon wall 1 detector . . . 17
1.16 Top view of the spectrometer highlighting how different particles can signal a trigger . . . 18
1.17 The two types of triggers (left is target pointing and right is energy loss) at COMPASS and an illustration of the coincidence matrix used to select events of interest . . . 18
1.18 The data acquisition steps at COMPASS . . . 20
1.19 The schematic of the CORAL reconstruction process . . . 21

List of Tables

Appendix A

Systematic Error Derivations

A.1 Systematic Error From Acceptance

For an asymmetry defined as

$$\mathrm{A}_{\alpha} = \frac{1}{\mathrm{P}} \frac{\alpha\sigma_L - \sigma_R}{\alpha\sigma_L + \sigma_R} \tag{A.1}$$

where α is an acceptance ratio. α is assumed to be close to unity therefore let

$$\alpha = 1 \pm 2 * \epsilon, \tag{A.2}$$

where ϵ is a small positive number. The asymmetry can therefore be written

$$\frac{1}{\mathrm{P}} \frac{(1 \pm 2 * \epsilon)\sigma_L - \sigma_R}{(1 \pm 2 * \epsilon)\sigma_L + \sigma_R} = \frac{1}{P} \frac{\sigma_L - \sigma_R \pm 2 * \epsilon * \sigma_L}{(\sigma_L + \sigma_R)(1 \pm \frac{2 * \epsilon * \sigma_L}{\sigma_L + \sigma_R})}. \tag{A.3}$$

From there Taylor expand the denominator to get

$$\mathrm{A}_{\alpha} \approx \frac{1}{\mathrm{P}} \frac{\sigma_L - \sigma_R \pm 2 * \epsilon * \sigma_L}{(\sigma_L + \sigma_R)} * (1 \mp \frac{2 * \epsilon * \sigma_L}{\sigma_L + \sigma_R}) \tag{A.4}$$

$$= \mathrm{A_N} \pm \frac{1}{\mathrm{P}} \frac{2 * \epsilon * \sigma_L}{\sigma_L + \sigma_R} \mp \mathrm{A_N} * \frac{2 * \epsilon * \sigma_L}{\sigma_L + \sigma_R} \mp \frac{1}{\mathrm{P}} \Big(\frac{2 * \epsilon * \sigma_L}{\sigma_L + \sigma_R} \Big)^2.$$

Assuming $\mathrm{A_N}$ is small and $\sigma_\mathrm{L} \approx \sigma_\mathrm{R}$

$$\mathrm{A}_{\alpha} \approx \mathrm{A_N} \pm \frac{\epsilon}{P}. \tag{A.5}$$

The true asymmetry can now be written

$$\mathrm{A_{N,systematic}} \approx \mathrm{A}_{\alpha} \mp \frac{\epsilon}{P}. \tag{A.6}$$

Including the $\frac{\epsilon}{P}$ term as an additive error and using standard error propagation the systematic error can be approximated as

$$\delta \mathrm{A_{N,systematic}} = \frac{\mid \alpha - 1 \mid}{2} \frac{1}{\mathrm{P}} + \frac{\delta_{\frac{\mid \alpha - 1 \mid}{2}}}{\mathrm{P}}. \tag{A.7}$$

A.2 Systematic Error From Left-Right Event Migration

Assuming the fraction of events miss-identified is γ and that the amount of miss-identified events reconstructed left equals the amount of outgoing events reconstructed right

$$\mathrm{A_{N,measure}} = \frac{1}{\mathrm{P}} \frac{(\mathrm{L} + \frac{\gamma}{2}\mathrm{N_{total}}) - (\mathrm{R} + \frac{\gamma}{2}\mathrm{N_{total}})}{(\mathrm{L} + \frac{\gamma}{2}\mathrm{N_{total}}) + (\mathrm{R} + \frac{\gamma}{2}\mathrm{N_{total}})} = \frac{1}{\mathrm{P}} \frac{\mathrm{L} - \mathrm{R}}{(\mathrm{L} + \mathrm{R}) * (1 + \gamma * \frac{\mathrm{N_{total}}}{\mathrm{L+R}})}, \tag{A.8}$$

where $\mathrm{N_{total}}$ is the total events measure, L is the true events measured to the left that should be measured left and R is the number of events measure to the right that should be measured to the right.

Assuming γ is a small percentage, the denominator can be Taylor expanded to give

$$\mathrm{A_{N,measure}} \approx \mathrm{A_N}\Big(1 - \gamma * \frac{\mathrm{N_{total}}}{\mathrm{L} + \mathrm{R}}\Big). \tag{A.9}$$

Including $\gamma \mathrm{A_{N,measure}}$ as an additive error and using standard error propagation the systematic error can be approximated as

$$\delta \mathrm{A_{N,systematic}} = \gamma * \mathrm{A_{N,measure}} + \gamma * \delta \mathrm{A_{N,measure}}. \tag{A.10}$$

References

[1] P. Abbon et al. The COMPASS experiment at CERN. *Nucl. Instrum. Meth.*, A577:455–518, 2007.

[2] A. Abragam and M. Goldman. Principles of dynamic nuclear polarisation. *Reports on Progress in Physics*, 41:395–467, 1978.

[3] V. Yu. Aleksakhin, Y. Bedfer, S. Gerasimov, and A. Yu. Korzenev. Geometrical event reconstruction in the COMPASS experiment. *Phys. Part. Nucl. Lett.*, 4:350–362, 2007. [Pisma Fiz. Elem. Chast. Atom. Yadra2007,no.4,588(2007)].

[4] Radja Boughezal, John M. Campbell, R. Keith Ellis, Christfried Focke, Walter Giele, Xiaohui Liu, Frank Petriello, and Ciaran Williams. Color singlet production at NNLO in MCFM. *Eur. Phys. J.*, C77(1):7, 2017.

[5] R. Fruhwirth. Application of Kalman filtering to track and vertex fitting. *Nucl. Instrum. Meth.*, A262:444–450, 1987.